HHS Public Access

Author manuscript

*Matrix Biol*. Author manuscript; available in PMC 2019 September 01.

Published in final edited form as:

*Matrix Biol*. 2017 January ; 57-58: 334–346. doi:10.1016/j.matbio.2016.08.009.

# A step towards clinical application of acellular matrix: a clue from macrophage polarization

**Astgik Petrosyan**[1], **Stefano Da Sacco**[1], **Nikita Tripuraneni**[1], **Ursula Kreuser**[2], **Maria Lavarreda-Pearce**[1], **Riccardo Tamburrini**[3], **Roger E. De Filippo**[1], **Giuseppe Orlando**[3], **Paolo Cravedi**[4], **Laura Perin**[1]

[1]GOFARR Laboratory for Organ Regenerative Research and Cell Therapeutics, Saban Research Institute, Children's Hospital Los Angeles; Department of Urology, University of Southern California, Los Angeles, CA, 90027, USA [2]Radboud Institute for Molecular Life Sciences, Department of Physiology, 6525 GA Nijmegen, The Netherlands [3]Department of General Surgery, Section of Transplantation, Wake Forest School of Medicine, Winston Salem, NC, 27157, USA [4]Renal Division, Department of Medicine, Icahn School of Medicine at Mount Sinai, One Gustave Levy Place, Annenberg Building New York, NY, 10029, USA

## Abstract

The outcome of tissue engineered organ transplants depends on the capacity of the biomaterial to promote a pro-healing response once implanted in vivo. Multiple studies, including ours, have demonstrated the possibility of using the extracellular matrix (ECM) of animal organs as platform for tissue engineering and more recently, discarded human organs have also been proposed as scaffold source. In contrast to artificial biomaterials, natural ECM has the advantage of undergoing continuous remodeling which allows adaptation to diverse conditions. It is known that natural matrices present diverse immune properties when compared to artificial biomaterials. However, how these properties compare between diseased and healthy ECM and artificial scaffolds has not yet been defined.

To answer this question, we used decellularized renal ECM derived from WT mice and from mice affected by Alport Syndrome at different time-points of disease progression as a model of renal failure with extensive fibrosis. We characterized the morphology and composition of these ECMs and compared their in vitro effects on macrophage activation with that of synthetic scaffolds commonly used in the clinic (collagen type I and poly-L-(lactic) acid, PLLA).

We showed that ECM derived from Alport kidneys differed in fibrous protein deposition and cytokine content when compared to ECM derived from WT kidneys. Yet, both WT and Alport renal ECM induced macrophage differentiation mainly towards a reparative (M2) phenotype, while artificial biomaterials towards an inflammatory (M1) phenotype. Anti-inflammatory properties of natural ECMs were lost when homogenized, hence three-dimensional structure of

***Corresponding Author:*** Laura Perin, PhD, 4661 Sunset Boulevard, Saban Research Institute, Children's Hospital Los Angeles, 90027, CA, USA. Phone: (323)3614584, FAX: (323)3613631, lperin@chla.usc.edu.

Disclosure Statement

No competing financial interests exist.

ECM seems crucial for generating an anti-inflammatory response. Together, these data support the notion that natural ECM, even if derived from diseased kidneys promote a M2 protolerogenic macrophage polarization, thus providing novel insights on the applicability of ECM obtained from discarded organs as ideal scaffold for tissue engineering.

**Keywords**

cell-matrix interactions; macrophages; renal extracellular matrix scaffolds (ECM)

## INTRODUCTION

Chronic kidney disease (CKD) has reached pandemic levels in the last decade [1]. Unfortunately, etiology and pathophysiology are unclear and treatment is often inadequate. Ideally, patients with CKD should receive therapies aimed at counteracting disease causes, as well as at enhancing endogenous repair mechanisms. However once patients reach end stage renal disease (ESRD) kidney transplantation is the optimal treatment option, but this opportunity is limited by an inadequate supply of transplantable grafts and by chronic toxicity of lifelong immunosuppression [2]. Therefore, many patients remain on dialysis instead of benefiting from a renal transplant, while the mortality rate of patients on the waiting list is progressively increasing [3].

Ex vivo organ/tissue bio-fabrication has been proposed as a strategy to increase the transplantable organ pool. So far, translation of tissue engineering technologies to clinical nephrology has been hampered – among other factors – by the lack of scaffolds capable of mimicking morphological and physiological characteristics of the kidney extracellular matrix (ECM) and securing a pro-healing response after transplantation [4].

In the past decade, acellular ECM scaffolds obtained from animal or human kidneys by decellularization have offered a valuable platform for kidney tissue engineering. The rationale for using natural scaffolds lies on the evidence that the ECM defines the physical and chemical interactions that control cellular physiology and fate and provides mechanical and structural support to cells and tissues [5]. While initial experiments focused on the rodent [4, 6–8], porcine [9,10]; and non-human primate ECMs [11–12], we proposed the use of human discarded kidneys as a source of acellular ECM scaffolds [4,13].

The ECM of human kidneys seems to be an extremely useful biomaterial for tissue engineering specifically because they maintain the framework of the innate vasculature intact, which is critical for implantation in vivo. Preliminary investigations have shown that such ECM can be successfully and consistently produced from discarded kidneys [4,13] that are devoid of immunogenic cell membrane proteins but retain their complex architecture, gross molecular composition and numerous growth factors (GFs) [14], which in turn provide a bioactive environment for stem cells cellular activity [15].

Shortly after implantation, scaffolds are infiltrated by immune cells that can modulate the inflammatory response via paracrine and autocrine signaling.

Among them, macrophages are shown to be actively involved in the initial immune response [16–18]. In particular, the delicate balance between their pro-inflammatory (M1) and reparative (M2) phenotype is key for the fate of the graft and functional regeneration in vivo [16–18].

In this work, we first studied structure and composition of kidney matrices derived from WT mice and from mice affected by Alport Syndrome, where a mutation in the collagen IVα5 gene causes an altered matrix deposition within the glomerulus with consequent renal fibrosis, chronic inflammation and kidney failure [19]. We investigated macrophage response induced by the healthy and diseased ECMs and compared with that obtained from artificial scaffolds of either collagen type 1 or poly-L-lactic acid (PLLA).

Overall, our data show that scaffolds derived from both healthy and diseased kidneys attenuate the pro-inflammatory macrophage phenotype when compared to synthetic material, providing the rationale for testing the use of scaffolds from discarded human donors as a preferred platform for tissue engineering.

## RESULTS

### Characterization of the mrECM in WT and Alport mice

Mice with Alport Syndrome used for these experiments start developing proteinuria, renal function impairment and renal fibrosis around 4 months of age and die on average at 7-8 months of age due to end stage renal diseases [Supplementary Fig. 1]. Therefore, we used ECM from Alport mice and WT controls taken at 5 and 7 months of age to recapitulate the abnormalities observed in advanced and terminal phases of renal failure.

Perfusion with Triton X-100 and multiple washes successfully decellularized 5 and 7 months Alport and WT murine kidneys. At gross observation, decellularized WT kidneys appeared translucent with evident vasculature outlines while Alport kidneys appeared smaller in size and opaque (Fig. 1A). H&E, PAS and Masson Trichrome staining of the WT mrECM showed maintenance of renal morphology such as glomeruli, vasculature and renal tubules during the time of analysis (Fig. 1B,D; Supplementary Fig. 2). On the contrary, Alport mrECM (starting at 5 months) showed variation in deposition of matrix (Supplementary Fig. 2B,F) and by 7 months demonstrated disorganized and fibrotic glomeruli with dense fibrotic depositions as shown by PAS and Masson Trichrome staining (Fig. 1C,E; Supplementary Figure 2D,H). The presence of fibrous proteins like collagen I, collagen IVα½ and fibronectin, is highly elevated in Alport mrECM compared to WT with predominant localization in the glomeruli (Fig. 2A–L; Supplementary Fig. 2I–J); indeed these mice present high glomerulosclerosis, interstitial fibrosis and macrophages infiltration as previously published [20]. Further analysis of ultra-thin epoxy resin by transmission electron microscopy (TEM) showed that the basement membranes (including the glomerular one) are highly modified in Alport mrECM compared to WT mrECM at 7 months of age (Fig. 3A–B).

### Cytokines analysis in WT and Alport mrECM

To analyze cytokine expression of WT and Alport mrECM, we performed a cytokine array analysis (Fig. 3C–D, Supplementary Fig. 3). Both matrices presented cytokines that are involved in both pro- and anti-inflammatory processes. By and large, Alport mrECM expressed higher levels of cytokines, with Reg3G, resistin, TIM-1/KIM-1 and DPPIV/CD26 being significantly different compared to the WT mrECM.

### Macrophage survival and proliferation on WT and Alport mrECM and effect of 3D-structure of mrECM on macrophage differentiation

We compared the adherence, survival and proliferation of macrophages on WT and Alport mrECM. At 5 days after seeding, macrophages were present on both mrECMs and localized in various compartments including tubules, interstitial space, glomeruli and vasculature (Fig. 4A–B). Intriguingly, the number of macrophages augmented from day 1 to day 5 in response to both mrECM, (Fig. 4C, Supplementary Fig. 4). Statistically significant number of macrophages adhered onto Alport mrECM after 5 days compared to 24hrs Alport mrECM, while no significant difference was observed between the number of cells on WT vs Alport mrECM after 5 days of seeding (Fig. 4C). Interestingly, macrophages seeded on both matrices presented high cellular turnover as indicated by increased staining for proliferative and apoptotic markers PCNA and BAX after 5 days compared to 24hrs after seeding (Supplementary Fig. 4).

To test the effect of 3D-structure of ECM on macrophage differentiation, we started by studying the expression profile of genes characteristic of M1/M2 in cells exposed to WT or Alport ECM, TCP, TCP plus INF-γ/LPS, collagen type 1 or PLLA for 48hrs. Compared to control macrophages seeded on TCP, macrophages seeded on mrECM or mrECM for 48hrs had lower expression of CD80 mRNA while CD80 in both collagen type 1 and PLLA did not decrease . Although the expression of mRNA for NOS2 was higher in macrophages seeded on both matrices compared to TCP, the mRNA level of NOS2 in macrophages seeded with mrECM was similar to that stimulated with INF-γ/LPS and significantly higher than macrophages seeded on mrECM (Fig. 4D). Macrophages cultured on TCP with INF-γ/LPS had significant higher levels of NOS2 mRNA ($p<0.005$) compared to that seeded on mrECM or collagen type 1 and PLLA. No significant differences were noted between macrophages seeded on Alport or WT mrECM.

Next we investigated if release of cytokines and growth factors embedded in the mrECM after homogenization impacts macrophage phenotype regardless of the 3D-structure of ECM. Homogenized Alport and WT mrECM had lower expression of CD86 mRNA but overall produced similar polarization effect to that stimulated by INF-γ/LPS and significantly different from that of macrophages exposed to non-homogenized ECM (Fig. 4D). Interestingly, both collagen type 1 and PLLA caused a decrease in CD150 mRNA expression compared to natural matrices. Overall, these data support that both healthy and diseased mrECM promote M2 phenotype differentiation, but only when ECM structure is intact.

### Phenotypic profile of macrophages after exposure to mrECM or synthetic biomaterial

To evaluate the immune properties of mrECM (WT or Alport) or artificial biomaterials (collagen type 1 or PLLA) on macrophage differentiation, we evaluated their M1 (CD80 and CD86) and M2 (CD150 and IL10R1) marker expression, in addition to CD64, by flow cytometry at 48hrs and 72hrs after seeding (Fig. 5 and Supplementary Fig. 5–7). We used macrophages seeded on tissue culture plates (TCP) with no stimulation and macrophages stimulated with INF-γ/LPS as negative and positive control, respectively. Macrophage phenotype after 48 or 72hrs seeding on synthetic material did not differ from that of cells seeded on TCP. In contrast, mrECM (both WT and Alport) induced a loss of CD80 (M1 marker) compared to unstimulated cells at 48hrs, which was more pronounced after 72hrs and was significantly lower compared to artificial biomaterials (Fig. 5E). Macrophages seeded on WT mrECM also had a significant increase in expression of M2 marker, CD150 (Fig. 5F), compared to unstimulated cells and cells seeded on collagen type 1 after 72 hrs. Expression of IL-10R1 and CD64 did not change across different seeding conditions (Fig. 5A–D and Fig. 5G). Altogether, these data provide evidences that macrophages seeded on either Alport or WT mrECM undergo a shift towards a M2 phenotype, as supported by reduced expression of M1 marker CD80 and increased expression of M2 marker CD150.

## DISCUSSION

Acellular ECM scaffolds represent a valuable platform for the bioengineering of transplantable organs, including the kidney [10, 21–22]. We have previously demonstrated that human renal ECM scaffolds maintain the structural complexities and biochemistry similarly to kidneys before decellularization [13–15]. The innate ECM is very dynamic and unique in physical, biochemical and biomechanical properties; it is extensively remodeled during the entire life of the organism and plays a critical role in maintenance of tissue homeostasis [23–24]. In the present report we showed that, compared to synthetic material, ECM derived from both normal and diseased kidneys have anti-inflammatory effects that could be important for optimization of scaffold engraftment.

Any implantable biomaterial, including the ECM, has the capability of stimulating macrophage recruitment, activation and maturation [25]. Therefore macrophage biological activity is crucial in directing implant success. Macrophages present two major “activation” states [26–27]; classically activated M1 macrophages (expressing CD80, CD86, NOS2, CCL2) tend to elicit chronic inflammation and tissue injury whereas the alternatively activated macrophages M2 (CD150, IL10R1) tend to resolve inflammation and facilitate wound healing [28–29]. Even if this classification in M1 or M2 phenotype is without any doubts a simplification of the in vivo reality and different subclasses for M2 or M1 phenotypes do exist and present different roles during repair and regeneration [30], the use of M1 and M2 is widely accepted as general distinction between macrophages with pro or anti healing capability.

Macrophages are responsible for inflammation resolution by production of high levels of matrix remodeling factors (MMPs, TIMPs) and are potent mediators of the immune-system activity through secretion of chemoattractants (such as IL-6, MCP-1, MIP-1b) to attract and recruit other inflammatory cells [31–32]. In general, during immune response there is

activation of all macrophage subtypes, initially driven by classically activated macrophages, which later subsides to alternatively activated (regulatory and wound-healing) macrophages for resolution [28, 33–35]. Improper activation of macrophage subtypes may lead to impaired wound healing with formation of excessive fibrosis and biomaterial encapsulation, thus causing rejection of the implant [16]. Therefore, the interplay of macrophage subtypes in a specific sequential temporal order is crucial for successful biomaterial implantation [30].

Previous studies showed that ECM obtained from healthy organs promote a M2 phenotype differentiation, while synthetic materials promote a M1 differentiation [36–38]. Interestingly, synthetic materials such as poly-propylene surgical meshes coated with ECM also show a reduced pro-inflammatory M1 response [37–38] since the coating alleviates the chronic inflammatory response and scar tissue formation characteristic of polypropylene [39].

In clinical setting, however, the human ECM that would be used for tissue engineering will be obtained from organs non suitable for transplantation. Therefore, it is of crucial importance to understand whether the same protolerogenic properties previously observed for healthy ECM extend to diseased ECMs. To this end, we used an established mouse model of chronic kidney disease (Alport Syndrome) with well-defined fibrosis and chronic inflammation to determine whether ECM derived from these kidneys would elicit different macrophage reactions compared to healthy ECM and synthetic scaffolds.

We first documented differences in structure and matrix composition between healthy and diseased ECMs. Thereafter, we compared cytokine and growth factor composition between healthy and diseased ECMs. Both the Alport and WT renal ECM expressed important pleotropic cytokines involved in tissue homeostasis and inflammation, including amongst others, chemokine (C-C motif) ligands (CCL3, CCL5, CCL6, CCL12) involved in the recruitment of immune cells [40], pro-/anti-angiogenic agents (VEGF, PDGF-BB, endostatin) [41], proinflammatory (IL1α, CD40, IL7) and anti-inflammatory molecules (IL4, IL10) [42,43], and mediators of matrix remodeling agents (MMP-2) [44]. In addition, both ECMs contained macrophage growth factors with anti-inflammatory and pro-inflammatory effects (G-CSF, GM-CSF) [45,46,].

Though most analyzed cytokines trended higher in Alport ECM, only Resistin, TIM-1/KIM-1, DPPIV/CD26, and Reg3G (regenerating islet-derived protein 3 gamma) reached statistical significance. Resistin, KIM-1 and DPPIV/CD26 have been associated with proinflammatory functions and are reported to be increased in chronic kidney diseases [47–50]. Resistin is secreted mainly by adipose tissue and increases both the expression of ICAM-1 and VCAM-1 by endothelial cells and monocyte adhesion to endothelial cells via p38MAPK-dependent pathways [48]. TIM-1/KIM-1 is a type 1 transmembrane protein, associated with increased macrophage production of nitric oxide, pro-inflammatory cytokines like TNF-α and IL-6 along and anti-inflammatory cytokines like IL-10 [49]. DPPIV/CD26 is a co-stimulatory molecule as well as a protease highly expressed on T cells. It functions as a T cell activating molecule and its soluble form may originate from endothelial or epithelial cells and from circulating leukocytes [50–51].

In contrast to the previous molecules, Reg3G has protolerogenic effects. Addition of Reg3G to prestimulated RAW 264.7 or primary macrophages has been shown to enhance M2 polarization through the activation of STAT3 signaling pathway [52] . Reg3G is also implicated in angiogenesis and prevention of cell apoptosis, both significant functions for tissue engineering.

Importantly, despite the different expression of cytokines and growth factors with mixed immune function between healthy and diseased mrECM, no variation was observed in their capacity to promote M2 macrophage polarization compared to synthetic matrices. Of note, both healthy and diseased ECMs promoted macrophage proliferation and expansion, which could be of major importance in controlling the immune response in vivo.

We also tested the importance of 3D-structure of ECMs on macrophage polarization by exposing cells to intact versus homogenized ECMs. The expression of mRNA for markers typical of M1 polarization (NOS2) in macrophages that were exposed to homogenized mrECM, was significantly different from that obtained with non-homogenized ECMs and similar to the one of cells exposed to INF-γ/LPS. These data strongly indicate that maintenance of the 3D-structure of the ECM (or the reduced access to embedded cytokines which would be favored by homogenization) is vital for reduced macrophage activation in both, diseased and healthy ECM. When this 3D-structure is lost, M1 polarization is favored instead thus further indicating the importance and the use of structurally preserved ECMs for in vivo transplantation.

The difference in macrophages response between homogenized and intact ECM could also depend on the type of organ from which the ECM is derived [53]. Meng et al. have shown that diverse tissue sources promote different macrophage responses [54]. For example, solubilized bladder ECM that contains hyaluronic acid (HA), unlike brain ECM, suppresses the traditional pro-inflammatory response and promotes an M2 phenotype [54]. Even if kidney ECM, similarly to bladder ECM, contains an even distribution of HA within the cortex and medulla [55], when homogenized, it promotes a M1 macrophage response comparable to that observed after stimulation with INF-γ/LPS. Therefore, we speculate that within the renal ECM there might exist a diverse organization (and composition) of basement membranes that, when disturbed, can promote a stronger M1 response.

In the US, more than 2,600 kidneys initially procured for transplant purposes are discarded every year due to severe biopsy-proven damage, anatomical anomalies or prolonged ischemia time [13, 56]. Our data support the idea that these organs may become a valuable source of ECM scaffolds for organ bioengineering. Of note, the present experiments proved the concept that although differences in fibrous protein deposition or cytokine expression between healthy and diseased kidneys exist, these variations do not account for prompting a positive M2 phenotype when macrophages are seeded on a healthy ECM.

Interestingly, our data confirm that ECM scaffolds are remarkably bioactive. In fact, we have previously shown that ECM scaffolds obtained from human kidneys [13] and pancreas [57] do trigger a strong angiogenic response when seeded within the corion allantoic membrane.

Moreover, we have observed that pancreas ECM promotes conversion of naïve $CD4^+$ T cells into Treg [57].

Our studies are limited by their in vitro nature and will need in vivo validation to understand the complexity of the host response to transplantable biomaterials. Herein, we utilized a genetic chronic kidney disease model, and it is difficult to assess if the same results apply to other diseased kidney models. Nevertheless, these results support the notion that discarded kidneys may serve as viable biomaterial capable of promoting a pro-healing immune response. Additionally, the use of ECM derived from diseased organs has the potential to be generalized beyond our current application to the kidney, since our findings can ultimately be applied to other organ systems, like for example the pancreas, lung and heart [58–59], so establishing new models for the treatment of organ failure by advancing the field of tissue engineering and scaffold fabrication.

## MATERIALS AND METHODS

### Kidney Decellularization

All animal studies were performed in adherence to the National Institutes of Health Guide for the Care and Use of Laboratory Animals and according to the protocols and guidelines of the Institutional Animal Care and Use Committee at Children's Hospital Los Angeles.

C57BL/6J WT and Alport mice (B6.Cg-Col4α5tm1Yseg/J, stock #006283) were purchased from Jackson Laboratory. Renal ECM was obtained from: 1. WT at 5 (n=23) and 7 (n=23) months of age and 2. Alport mice at 5 (n=23) and 7 (n=23) month. Decellularized kidneys were used for the following experiments: 1. Histology, homogenization, TEM analysis [WT (n=10) and Alport (n=10)], 2. RNA analysis [WT (n=4) and Alport (n=4)] 3. Cytokines [ WT (n=3) and Alport (n=3)] , 4. Flow cytometry analyses [WT (n=6) and Alport (n=6)].

To obtain kidneys, mice were anesthetized with ketamine–xylazine solution and perfused with PBS (Gibco/Invitrogen) through the left ventricle followed by 3% Triton X-100 (Sigma-Aldrich). After removal, the kidneys were incubated in 3% Triton X-100 (Sigma-Aldrich) at 4°C for 5 days and than placed in agitation for 14 days with continuous solution changes and 3 washes in DI water biweekly. Specimens were then incubated in 4% sodium deoxycholate (Sigma-Aldrich), and kept in agitation for 5 hrs followed by rinses. Thereafter, they were placed in sterile filtered 1 M NaCl (Sigma-Aldrich) with sterile 30 mg/mL porcine pancreatic DNase (Sigma-Aldrich, for 4 hrs at room temperature and rinsed. Following the final rinse, specimens were sterilized with 100 μg/ml Primocin (Invivo Gene) for 30 min in agitation followed by 2 hrs of washing with PBS. DAPI and H&E staining were used to confirm the absence of cellular and nuclear material.

### Macrophage isolation and seeding on mrECM and synthetic biomaterials

Macrophages were isolated from C57BL/6J mice ($n$=25) as previously described [60]. Briefly, 1 mL of a 4% sterile thioglycollate solution (Brewer thioglycollate medium, DIFCO) was injected intra-peritoneally under isoflurane and mice were sacrificed with CO2 administration after 4 days. After harvesting, macrophage were further purified using the magnetic activated cell sorting (Monocyte Isolation Kit (BM) Miltenyi Biotech) according to

the manufacturer's instructions (purity >95%) and cultured in 94.8% complete RPMI, 5% heat inactivated FBS, (Gibco/BRL) and 0.02% Primocin (InvivoGen). Decellularized WT and Alport mrECM were cross sectioned to a thickness of 300 μm using a vibratome and approximately $1\times10^6$ macrophages were cultured in RPMI1640 Medium and 5% FBS in a 24 well tissue culture plate for the in vitro cultures.

48hr and 72hr cell cultures (in triplicate) were established for the following groups: 1. Non-activated macrophages, 2. INF-γ/LPS (150 U/ml Cellsciences, and 30 ng/ml, Sigma-Aldrich)-activated macrophages, 3. Non-activated macrophages plus 7 months WT mrECM, 4. Non-activated macrophages plus 7 months Alport mrECM, 5. Non-activated macrophages on collagen type I (rat tails, Corning in 0.02N acetic acid) coated plates, 6. Non-activated macrophages plus $1cm^3$ poly-L-lactic acid (PLLA, Biofelt; 83.5%. porosity 12.1uM mean size, provided by Dr Orlando, Wake Forest University) biomaterial. Whole WT and Alport mrECM were mechanically homogenized using a VWR® 200 homogenizer in 500 μl of media and frozen. After freezing samples were thawed and centrifuged at 300g for 10 min and used for *in vitro* experiments. Cells were primed with INF-γ for 12 hours prior to administration of LPS.

## RNA isolation and Real-Time PCR

RNA was extracted from experimental groups using the Qiagen RNeasy kit (Qiagen) and following the manufacturer's instructions.

Quantitative real-time PCR for NOS2, CCL2, CD80, CD86, CD150 was carried out using a Roche Light Cycler 480. Real-time PCR conditions were as follows: 90°C for 10 minutes, 60°C for 10 seconds, and 72°C for 1 second with the analysis of the fluorescent emission at 72°C. Thirty-five cycles were performed for each experiment. qRT-PCR $RT^2$ First Strand Kit [SABiosciences] was used to convert mRNA to cDNA. This cDNA was then added to the SA biosciences $RT^2$ SYBR Green qPCR Master Mix. Each sample was used to perform quantitative gene expression analysis on specific genes (Supplementary Table 1) All steps were done according to the manufacturer's protocol for the Roche Light Cycler 480. CP scores where collected and fold changes where calculated.

## Paraffin embedding and staining

Samples were fixed with 10% formalin (Azer Scientific) in PBS and then dehydrated through alcohol gradients. Tissues were cleared through 2 changes of toluene (Sigma-Aldrich) 30 min each and immersed in paraffin/toluene followed by two changes of 100% paraffin for one hour each and 100% paraffin O/N. Finally, samples were submerged in wax and embedded in a paraffin block stored in 4°C and further sectioned. 5 μm thick sections of mrECM (Rotary Microtome-Leica, Rotary Microtome RM2235) were deparaffinized and rehydrated in alcoholic gradients for histology.

## Immunohistochemistry and Immunofluorescence

Haematoxylin and eosin (Sigma-Aldrich) staining was performed by 90 seconds of incubation in haematoxylin followed by 30 seconds of incubation in eosin. Trichrome Masson staining samples were fixed with Bouin's solution (Sigma-Aldrich) for 15 min at

56°C followed by Wiegerts iron haematoxylin (Sigma-Aldrich) for 5 min, then a trichrome kit (Sigma-Aldrich) and finally incubated with 1% acetic acid for 2 min. A bright field microscope was used to take 10x & 20x images. Periodic Acid-Schiff reagent (Sigma-Aldrich) was used to preform PAS staining following standard protocols.

Immunofluorescence analyses of cell count were visualized with DAPI (Vector Laboratories Burlingame). Minimum of 60 10x bright field microscopic images (Leica DM5500 B Microscope System) per experimental group were counted for positive expression of DAPI. ImageJ software determined cell count. Immunofluorescence analysis was conducted by 1hr incubation with primary antibodies collagen IVα1/α2, collagen I, fibronectin, PCNA and Bcl-associated X protein (Bax), followed by a 30 min incubation with secondary anti-mouse or anti-rabbit Alexa Fluor 555 (Life Technologies Grand Island, NY, 1:500) See Supplementary Table 2 for antibody dilution. DAPI mounting (Vector Laboratories) was used to visualize samples with a Leica DM5500 B Microscope System.

### Evaluation of albumin and creatinine in WT and Alport mice

Urine samples from WT mice (n=5) and Alport mice (n=8) were collected overnight from single mice housed in metabolic cages (Hatteras Instruments, #CCS2000). Urine samples were collected at different time points during disease progression (2, 4 and 6 months of age). Blood samples (30 μL) from all experimental groups were collected into plasma separation tubes with lithium heparin. The urine albumin-to-creatinine ratio was determined using an ELISA for albuminuria (Mouse Albumin ELISA kit, # E-90AL Immunology Consultants Laboratory ) and quantitative colorimetric assay kit for urine and serum creatinine (QuantiChrom Creatinine Assay kit, #DICT-500 Bioassay Systems) was performed following manufacturers' protocols.

### Flow cytometry analysis

The expression of CD80, CD86, CD64, CD150 and IL 10R1 markers was analyzed by flow cytometry (Table 2). Flow cytometry analysis was performed in quadruplicate for all experimental groups at 48 hrs and 72 hrs, along with macrophages unstimulated or primed with INF-γ and activated with LPS). Data acquisition and analysis of all samples by flow cytometry were performed with BD FACSDiva 5.0.1 flow cytometry system and BD FACSDiva5.1.3 software.

### Extracellular matrix cytokine analysis

mrECM from whole 3 WT kidneys and 3 Alport kidneys at 7 months were used to evaluate cytokine retention and experiments were performed according to manufacturer protocols. Samples were homogenized in 500 μl of PBS with protease inhibitors and stored at (−80°C). To perform cytokine measurements, samples were thawed and centrifuged for 5 min at 10,000g. Supernatants were then collected and assayed immediately. Protein expression profiles were obtained using a Mouse XL Cytokine Array Kit, a membrane-based sandwich immunoassay that measures 111 mouse cytokines and growth factors simultaneously, following manufacturer protocols. Briefly, samples were incubated overnight with the nitrocellulose membranes after a blocking step, washed to remove nonspecific proteins, and biotin-labeled detection antibodies were added. The cytokine-antibody-biotin complexes

were visualized using chemiluminescent detection reagents. Average chemiluminescent intensity was obtained by measuring pixel density.

### Transmission electron microscopy

mrECM from 7-month old WT (n=3) and Alport (n=3) animals were fixed with 2% glutaraldehyde (Sigma-Aldrich) in sodium phosphate buffer. Samples were then placed in 1% osmium tetroxide (Sigma-Aldrich) for 1 hour and dehydrated in 50%, 70%, 90%, 95%, 100%, ethanol and propylene oxide (Sigma-Aldrich) for 10 min each. Samples were then infused with an epoxy resin mixture (Eponate 12 resin) (TED PELLA Inc.). Ultra-thin sections were collected on copper grids (Electron Microscopy Science. Hatfield), and sections were stained using 10% uranyl acetate (Electron Microscopy Science) in 50% methanol (Thermo Fisher Scientific) and a modified Sato lead stain (Pathology Laboratory, Children's Hospital Los Angeles,). A Morgagni 268 electron microscope (FEI) was used for picture acquisition with the assistance of the Pathology Laboratory, Children's Hospital Los Angeles.

### Statistics

All *in vitro* experiments were performed in triplicate at the minimum for all the experimental groups. Results are presented as mean ± SEM. Statistical differences between groups was assessed using a student T-test, One-Way Anova and Two-Way Anova using PRISM 7 software. Tukey's multiple comparison tests were used for flow cytometer, cell count and RNA multiple comparisons. Sidak's multiple comparison tests were used for mouse XL cytokine array multiple comparisons. A p value lower than or equal to 0.05 was considered significant and expressed as * for $p<0.05$ , ** for $p<0.005$, *** for $p<0.001$ and **** for $p<0.0001$.

## Supplementary Material

Refer to Web version on PubMed Central for supplementary material.

## Acknowledgments

We thank Dr H. Shimada and Minerva Mongeotti for help with the transmission electron microscopy protocols and interpretation of the data. We thank the GOFFAR Foundation for financial support, the California Institute for Regenerative Medicine (CIRM, Da Sacco S) and the Nora Baart foundation and from the Dutch kidney foundation (Kreuser U).

## REFERENCES

1. Liyanage T, Ninomiya T, Jha V, Neal B, Patrice HM, Okpechi I, Zhao MH, Lv J, Garg AX, Knight J, Rodgers A, Gallagher M, Kotwal S, Cass A, Perkovic V, Worldwide access to treatment for end-stage kidney disease: a systematic review, Lancet. 385 (2015) 1975–82. [PubMed: 25777665]
2. Orlando G, Soker S, Stratta RJ, Organ bioengineering and regeneration as the new Holy Grail for organ transplantation, Ann Surg. 258 (2013) 221–32. [PubMed: 23782908]
3. Data available from: U.S. Department of Health and Human Services. http://optn.transplant.hrsa.gov/.
4. Petrosyan A, Zanusso I, Lavarreda-Pearce M, Leslie S, Sedrakyan S, De Filippo RE, Orlando G, Da Sacco S, Perin L, Decellularized Renal Matrix and Regenerative Medicine of the Kidney: A Different Point of View, Tissue Eng Part B Rev. 22 (2016) 183–92. [PubMed: 26653996]

5. Hynes RO, Extracellular matrix: not just pretty fibrils, Science. 326 (2009) 1216–19. [PubMed: 19965464]
6. Song JJ, Guyette JP, Gilpin SE, Gonzalez G, Vacanti JP, Ott HC, Regeneration and experimental orthotopic transplantation of a bioengineered kidney, Nat Med. 19 (2013) 646–51. [PubMed: 23584091]
7. Caralt M, Uzarski JS, Iacob S, Obergfell KP, Berg N, Bijonowski BM, Kiefer KM, Ward HH, Wandinger-Ness A, Miller WM, Zhang ZJ, Abecassis MM, Wertheim JA, Optimization and critical evaluation of decellularization strategies to develop renal extracellular matrix scaffolds as biological templates for organ engineering and transplantation, Am J Transplant. 15 (2015) 64–75. [PubMed: 25403742]
8. Ross EA, Abrahamson DR, St John P, Clapp WL, Williams MJ, Terada N, Hamazaki T, Ellison GW, Batich CD, Mouse stem cells seeded into decellularized rat kidney scaffolds endothelialize and remodel basement membranes, Organogenesis. 8 (2012) 49–55. [PubMed: 22692231]
9. Sullivan DC, Mirmalek-Sani SH, Deegan DB, Baptista PM, Aboushwareb T, Atala A, Yoo JJ, Decellularization methods of porcine kidneys for whole organ engineering using a high-throughput system, Biomaterials. 33 (2012) 7756–64. [PubMed: 22841923]
10. Orlando G, Farney AC, Iskandar SS, Mirmalek-Sani SH, Sullivan DC, Moran E, AbouShwareb T, De Coppi P, Wood KJ, Stratta RJ, Atala A, Yoo JJ, Soker S, Production and implantation of renal extracellular matrix scaffolds from porcine kidneys as a platform for renal bioengineering investigations, Ann Surg. 256 (2012) 363–70. [PubMed: 22691371]
11. Nakayama KH, Batchelder CA, Lee CI, Tarantal AF, Decellularized rhesus monkey kidney as a three-dimensional scaffold for renal tissue engineering, Tissue Eng Part A. 16 (2010) 2207–16. [PubMed: 20156112]
12. Nakayama KH, Lee CC, Batchelder CA, Tarantal AF, Tissue specificity of decellularized rhesus monkey kidney and lung scaffolds, PLoS One. 8 (2013) e64134. [PubMed: 23717553]
13. Orlando G, Booth C, Wang Z, Totonelli G, Ross CL, Moran E, Salvatori M, Maghsoudlou P, Turmaine M, Delario G, Al-Shraideh Y, Farooq U, Farney AC, Rogers J, Iskandar SS, Burns A, Marini FC, De Coppi P, Stratta RJ, Soker S, Discarded human kidneys as a source of ECM scaffold for kidney regeneration technologies, Biomaterials. 34 (2013) 5915–25. [PubMed: 23680364]
14. Peloso A, Petrosyan A, Da Sacco S, Booth C, Zambon JP, O'Brien T, Aardema C, Robertson J, De Filippo RE, Soker S, Stratta RJ, Perin L, Orlando G, Renal Extracellular Matrix Scaffolds From Discarded Kidneys Maintain Glomerular Morphometry and Vascular Resilience and Retains Critical Growth Factors, Transplantation. 99 (2015) 1807–16. [PubMed: 26018349]
15. Petrosyan A, Orlando G, Peloso A, Wang Z, Farney AC, Rogers J, De Filippo RE, Delario G, Willis CD, Stratta RJ, Soker S, Perin L, Understanding the bioactivity of stem cells seeded on ECM produced from discarded human kidneys, CellR4. 3 (2015) e1401.
16. Anderson JM, Rodriguez A, Chang DT, Foreign body reaction to biomaterials, Semin Immunol. 20 (2008) 86–100. [PubMed: 18162407]
17. Mosser DM, Edwards JP, Exploring the full spectrum of macrophage activation, Nat Rev Immunol. 8 (2008) 958–69. [PubMed: 19029990]
18. Brown BN, Ratner BD, Goodman SB, Amar S, Badylak SF, Macrophage polarization: an opportunity for improved outcomes in biomaterials and regenerative medicine, Biomaterials. 33 (2012) 3792–802. [PubMed: 22386919]
19. Rheault MN, Kren SM, Thielen BK, Mesa HA, Crosson JT, Thomas W, Sado Y, Kashtan CE, Segal Y, Mouse model of X-linked Alport syndrome, J Am Soc Nephrol. 15 (2004) 1466–74. [PubMed: 15153557]
20. Sedrakyan S, Da Sacco S, Milanesi A, Shiri L, Petrosyan A, Varimezova R, Warburton D, Lemley KV, De Filippo RE, Perin L, Injection of amniotic fluid stem cells delays progression of renal fibrosis, J Am Soc Nephrol. 23 (2012) 661–73. [PubMed: 22302195]
21. Badylak SF, Taylor D, Uygun K, Whole-organ tissue engineering: decellularization and recellularization of three-dimensional matrix scaffolds, Annu Rev Biomed Eng. 13 (2011) 27–53. [PubMed: 21417722]

22. Badylak SF, Weiss DJ, Caplan A, Macchiarini P, Engineered whole organs and complex tissues, Lancet. 379 (2012) 943–52. [PubMed: 22405797]
23. Müller U, Brändli AW, Cell adhesion molecules and extracellular-matrix constituents in kidney development and disease, J Cell Sci. 112 (1999) 3855–67. [PubMed: 10547347]
24. Kim SH, Turnbull J, Guimond S, Extracellular matrix and cell signalling: the dynamic cooperation of integrin, proteoglycan and growth factor receptor, J Endocrinol. 209 (2011) 139–51. [PubMed: 21307119]
25. Franz S, Rammelt S, Scharnweber D, Simon JC, Immune responses to implants - a review of the implications for the design of immunomodulatory biomaterials, Biomaterials. 32 (2011) 6692–709. [PubMed: 21715002]
26. Classen A, Lloberas J, Celada A, Macrophage activation: classical versus alternative, Methods Mol Biol. 531 (2009) 29–43. [PubMed: 19347309]
27. Nolan A, Kobayashi H, Naveed B, Kelly A, Hoshino Y, Hoshino S, Karulf MR, Rom WN, Weiden MD, Gold JA, Differential role for CD80 and CD86 in the regulation of the innate immune response in murine polymicrobial sepsis, PLoS One. 4 (2009) e6600. [PubMed: 19672303]
28. Ricardo SD, van Goor H, Eddy AA, Macrophage diversity in renal injury and repair, J Clin Invest. 118 (2008) 3522–30. [PubMed: 18982158]
29. Martinez FO, Gordon S, The M1 and M2 paradigm of macrophage activation: time for reassessment, F1000Prime Rep. 6 (2014) 13. [PubMed: 24669294]
30. Brown BN, Sicari BM, Badylak SF, Rethinking regenerative medicine: a macrophage-centered approach, Front Immunol. 5 (2014) 510. [PubMed: 25408693]
31. Jones JA, Chang DT, Meyerson H, Colton E, Kwon IK, Matsuda T, Anderson JM, Proteomic analysis and quantification of cytokines and chemokines from biomaterial surface-adherent macrophages and foreign body giant cells, J Biomed Mater Res A. 83 (2007) 585–96. [PubMed: 17503526]
32. Cohen HB, Mosser DM, Extrinsic and intrinsic control of macrophage inflammatory responses, J Leukoc Biol. 94 (2013) 913–9. [PubMed: 23964115]
33. Troidl C, Möllmann H, Nef H, Masseli F, Voss S, Szardien S, Willmer M, Rolf A, Rixe J, Troidl K, Kostin S, Hamm C, Elsässer A, Classically and alternatively activated macrophages contribute to tissue remodelling after myocardial infarction, J Cell Mol Med. 13 (2009) 3485–96. [PubMed: 19228260]
34. Mantovani A, Biswas SK, Galdiero MR, Sica A, Locati M, Macrophage plasticity and polarization in tissue repair and remodelling, J Pathol. 229 (2013) 176–85. [PubMed: 23096265]
35. Brown BN, Londono R, Tottey S, Zhang L, Kukla KA, Wolf MT, Daly KA, Reing JE, Badylak SF, Macrophage phenotype as a predictor of constructive remodeling following the implantation of biologically derived surgical mesh materials, Acta Biomater. 8 (2012) 978–87. [PubMed: 22166681]
36. Fishman JM, Lowdell MW, Urbani L, Ansari T, Burns AJ, Turmaine M, North J, Sibbons P, Seifalian AM, Wood KJ, Birchall MA, De Coppi P, Immunomodulatory effect of a decellularized skeletal muscle scaffold in a discordant xenotransplantation model, Proc Natl Acad Sci U S A. 110 (2013) 14360–5. [PubMed: 23940349]
37. Wolf MT, Dearth CL, Ranallo CA, LoPresti ST, Carey LE, Daly KA, Brown BN, Badylak SF, Macrophage polarization in response to ECM coated polypropylene mesh, Biomaterials. 35 (2014) 6838–49. [PubMed: 24856104]
38. Faulk DM, Londono R, Wolf MT, Ranallo CA, Carruthers CA, Wildemann JD, Dearth CL, Badylak SF, ECM hydrogel coating mitigates the chronic inflammatory response to polypropylene mesh, Biomaterials. 35 (2014) 8585–95. [PubMed: 25043571]
39. Grotenhuis N, Bayon Y, Lange JF, Van Osch GJ, Bastiaansen-Jenniskens YM, A culture model to analyze the acute biomaterial-dependent reaction of human primary macrophages, Biochem Biophys Res Commun. 433 (2013) 115–20. [PubMed: 23485466]
40. Burke ML, McManus DP, Ramm GA, Duke M, Li Y, Jones MK, Gobert GN, Temporal expression of chemokines dictates the hepatic inflammatory infiltrate in a murine model of schistosomiasis, PLoS Negl Trop Dis. 4 (2010) e598. [PubMed: 20161726]

41. Nicosia RF, Nicosia SV, Smith M, Vascular endothelial growth factor, platelet-derived growth factor, and insulin-like growth factor-1 promote rat aortic angiogenesis in vitro, Am J Pathol. 145 (1994) 1023–9. [PubMed: 7526691]
42. Zhang JM, An J, Cytokines, inflammation, and pain, Int Anesthesiol Clin. 45 (2007) 27–37. [PubMed: 17426506]
43. Carreno BM, Becker-Hapak M, Linette GP, CD40 regulates human dendritic cell-derived IL-7 production that, in turn, contributes to CD8(+) T-cell antigen-specific expansion, Immunol Cell Biol. 87 (2009) 167–77. [PubMed: 19002156]
44. Chen Q, Jin M, Yang F, Zhu J, Xiao Q, Zhang L, Matrix metalloproteinases: inflammatory regulators of cell behaviors in vascular formation and remodeling, Mediators Inflamm. 2013 (2013) 928315. [PubMed: 23840100]
45. Kitching AR, Ru Huang X, Turner AL, Tipping PG, Dunn AR, Holdsworth SR, The requirement for granulocyte-macrophage colony-stimulating factor and granulocyte colony-stimulating factor in leukocyte-mediated immune glomerular injury, J Am Soc Nephrol. 13 (2002) 350–8. [PubMed: 11805162]
46. Martins A, Han J, Kim SO, The multifaceted effects of granulocyte colony-stimulating factor in immunomodulation and potential roles in intestinal immune homeostasis, IUBMB Life. 62 (2010) 611–7. [PubMed: 20681025]
47. Dan S, Aditya P, Banerjee P, Bal C, Roy H, Banerjee I, Effect of chronic kidney disease on serum resistin level, Niger J Clin Pract. 17 (2014) 735–8. [PubMed: 25385911]
48. Axelsson J, Bergsten A, Qureshi AR, Heimbürger O, Bárány P, Lönnqvist F, Lindholm B, Nordfors L, Alvestrand A, Stenvinkel P, Elevated resistin levels in chronic kidney disease are associated with decreased glomerular filtration rate and inflammation, but not with insulin resistance, Kidney Int. 69 (2006) 596–604. [PubMed: 16395259]
49. Waanders F, van Timmeren MM, Stegeman CA, Bakker SJ, van Goor H, Kidney injury molecule-1 in renal disease, J Pathol. 220 (2010) 7–16. [PubMed: 19921716]
50. Varona A, Blanco L, Perez I, Gil J, Irazusta J, López JI, Candenas ML, Pinto FM, Larrinaga G, Expression and activity profiles of DPP IV/CD26 and NEP/CD10 glycoproteins in the human renal cancer are tumor-type dependent, BMC Cancer. 10 (2010) 193. [PubMed: 20459800]
51. Gorrell MD, Gysbers V, McCaughan GW, CD26: a multifunctional integral membrane and secreted protein of activated lymphocytes, Scand J Immunol. 54 (2001) 249–64. [PubMed: 11555388]
52. Folch-Puy E, REG3β contributes to the immunosuppressive microenvironment of pancreatic cancer, Oncoimmunology. 2 (2013) e26404. [PubMed: 24353919]
53. Sicari BM, Dziki JL, Siu BF, Medberry CJ, Dearth CL, Badylak SF, The promotion of a constructive macrophage phenotype by solubilized extracellular matrix, Biomaterials. 35 (2014) 8605–12. [PubMed: 25043569]
54. Meng FW, Slivka PF, Dearth CL, Badylak SF, Solubilized extracellular matrix from brain and urinary bladder elicits distinct functional and phenotypic responses in macrophages, Biomaterials. 46 (2015) 131–40. [PubMed: 25678122]
55. Dicker SE, Franklin CS, The isolation of hyaluronic acid and chondroitin sulphate from kidneys and their reaction with urinary hyaluronidase, J Physiol. 186 (1966) 110–20. [PubMed: 5914246]
56. Hosgood SA, Barlow AD, Dormer J, Nicholson ML, The use of ex-vivo normothermic perfusion for the resuscitation and assessment of human kidneys discarded because of inadequate in situ perfusion, J Transl Med. 13 (2015) 329. [PubMed: 26474973]
57. Peloso A, Urbani L, Cravedi P, Katari R, Maghsoudlou P, Fallas ME, Sordi V, Citro A, Purroy C, Niu G, McQuilling JP, Sittadjody S, Farney AC, Iskandar SS, Zambon JP, Rogers J, Stratta RJ, Opara EC, Piemonti L, Furdui CM, Soker S, De Coppi P, Orlando G, The Human Pancreas as a Source of Protolerogenic Extracellular Matrix Scaffold for a New-generation Bioartificial Endocrine Pancreas, Ann Surg. (2015).
58. Guyette JP, Charest JM, Mills RW, Jank BJ, Moser PT, Gilpin SE, Gershlak JR, Okamoto T, Gonzalez G, Milan DJ, Gaudette GR, Ott HC, Bioengineering Human Myocardium on Native Extracellular Matrix, Circ Res. 118 (2016) 56–72. [PubMed: 26503464]

59. Ren X, Moser PT, Gilpin SE, Okamoto T, Wu T, Tapias LF, Mercier FE, Xiong L, Ghawi R, Scadden DT, Mathisen DJ, Ott HC, Engineering pulmonary vasculature in decellularized rat and human lungs, Nat Biotechnol. 33 (2015) 1097–102. [PubMed: 26368048]

60. Li YM, Baviello G, Vlassara H, Mitsuhashi T, Glycation products in aged thioglycollate medium enhance the elicitation of peritoneal macrophages, J Immunol Methods. 201 (1997) 183–8. [PubMed: 9050940]

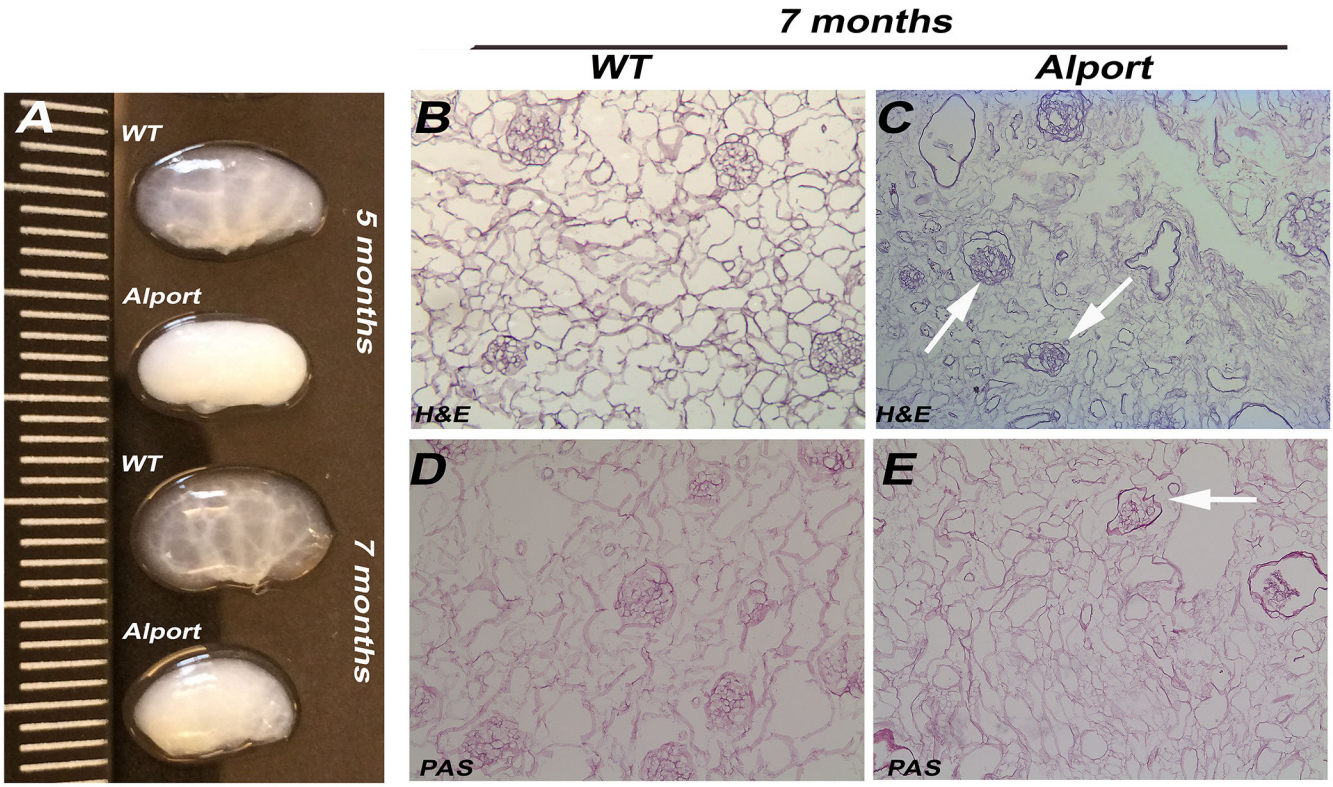


**Figure 1: Histological characterization of mrECM from WT and Alport mice**

**A**. Representative images of WT and Alport kidneys at 5 and 7 months of age. Alport kidneys appear smaller in size and opaque while WT kidneys appear translucent (measurement in cm). **B-E**. Representative bight field images of H&E (**B-D**) and PAS staining (**C-E**) of WT mrECM at 7 months (**B,D**) and Alport mrECM at 7 months (**C,E)** showing differences in matrix deposition between later stage disease and WT matrices. Alport matrix showed disorganization of the glomerular structure (arrows) and vessels. Magnification 20x.

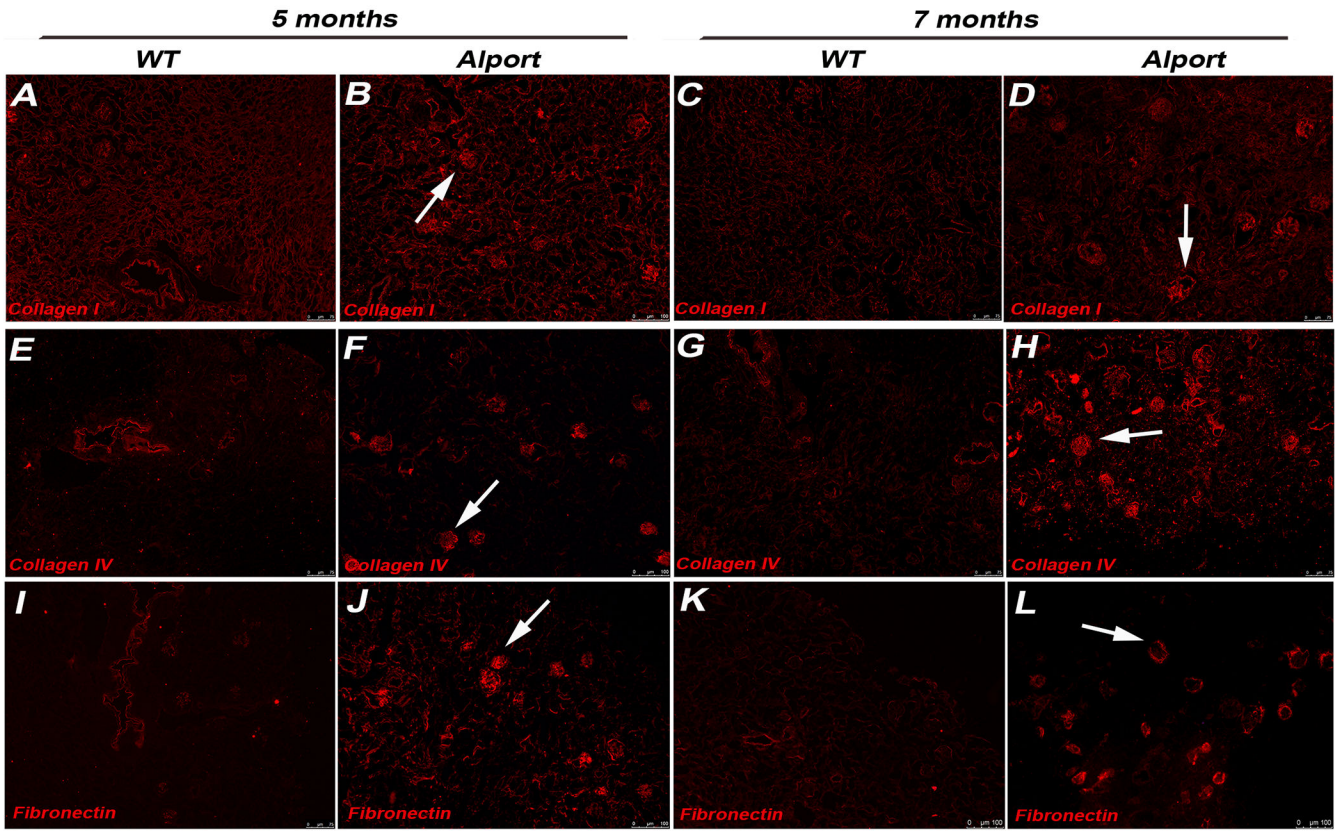


**Figure 2: Immune-fluorescent staining for collagen I, collagen IVα1/α2 and fibronectin of mrECM from WT and Alport mice**

Representative immune-fluorescence images for collagen I (**A-D**), collagen IV α1/α2 (**E-H**), and fibronectin (**I-L**) staining of WT mrECM at 5 months (**A,E,I**) and 7 months (**C,G,K**) and Alport mrECM at 5 months (**B,F,J**) and 7 months (**D,H,L**) of age. Full decellularization of mrECM from both WT and Alport mice is proved by the absence of DAPI signal. Glomeruli of Alport mrECM present strong expression of collagen I (**D**, arrow) and collagen IVα1/α2 (**H**, arrow) and fibronectin (**L**, arrow) which is very evident at 7 months of age. Magnification: 10x, nuclei stained in DAPI, blue.

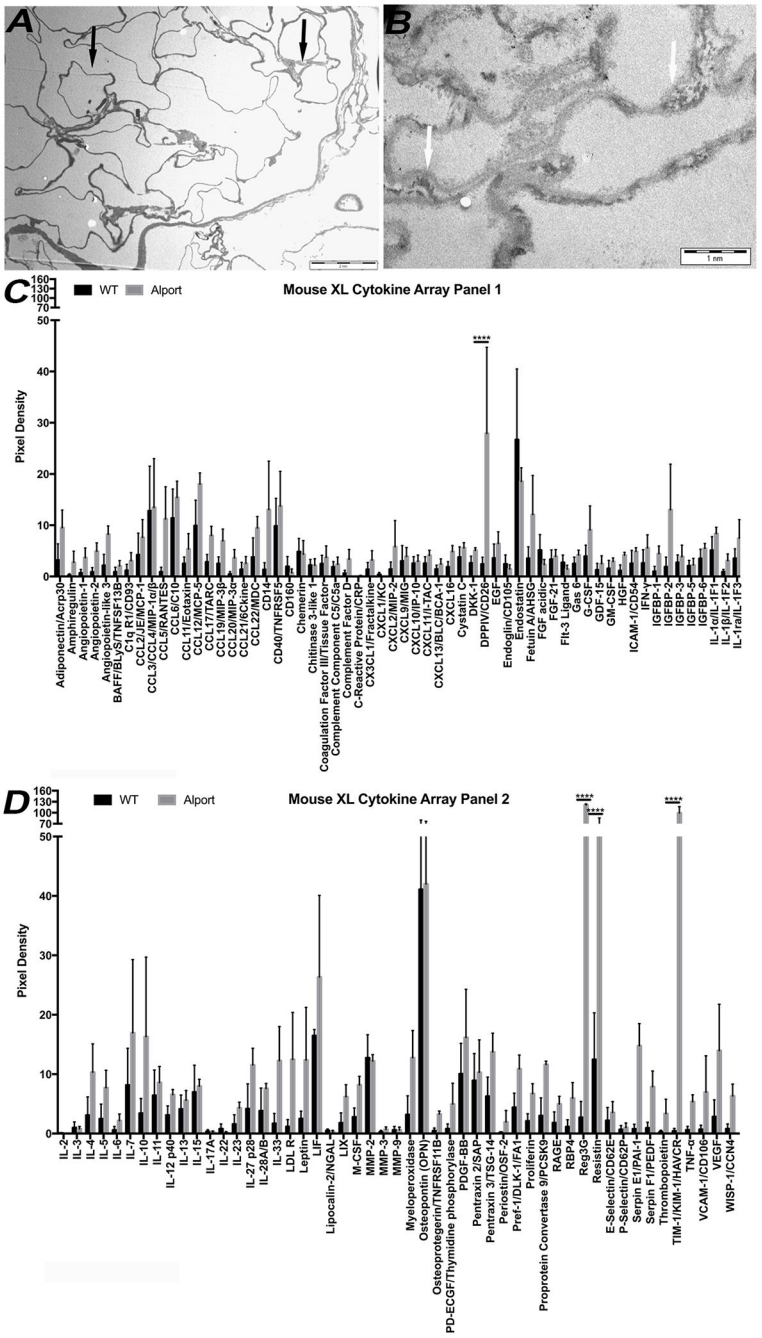


**Figure 3: Transmission electron microscopy evaluation and cytokine expression analysis of WT and Alport mrECM at 7 months of age.**

**A-B**. Representative electron transmission microscopy images of WT mrECM at 7 months (**A**) and Alport mrECM at 7 months (**B**) showing ultrastructural differences in membrane deposition between WT and Alport (arrow) and severe thinning and splitting of glomerular basement membrane (**B,** arrow) in Alport mrECM. Scale bar is reported in **A** and **B.**

**C-D.** Mouse cytokine array analysis confirming the presence of numerous cytokines within WT and Alport mrECM at 7 months of age upon homogenization. Only 4 out of 111

cytokines (CD26, REG3G, resistin and KIM1) showed to be statistically significantly different between WT and Alport samples, with Alport showing higher expression for each of them (*$p<0.05$, **$p<0.005$, ***$p<0.001$, ****$p< 0.0001$).

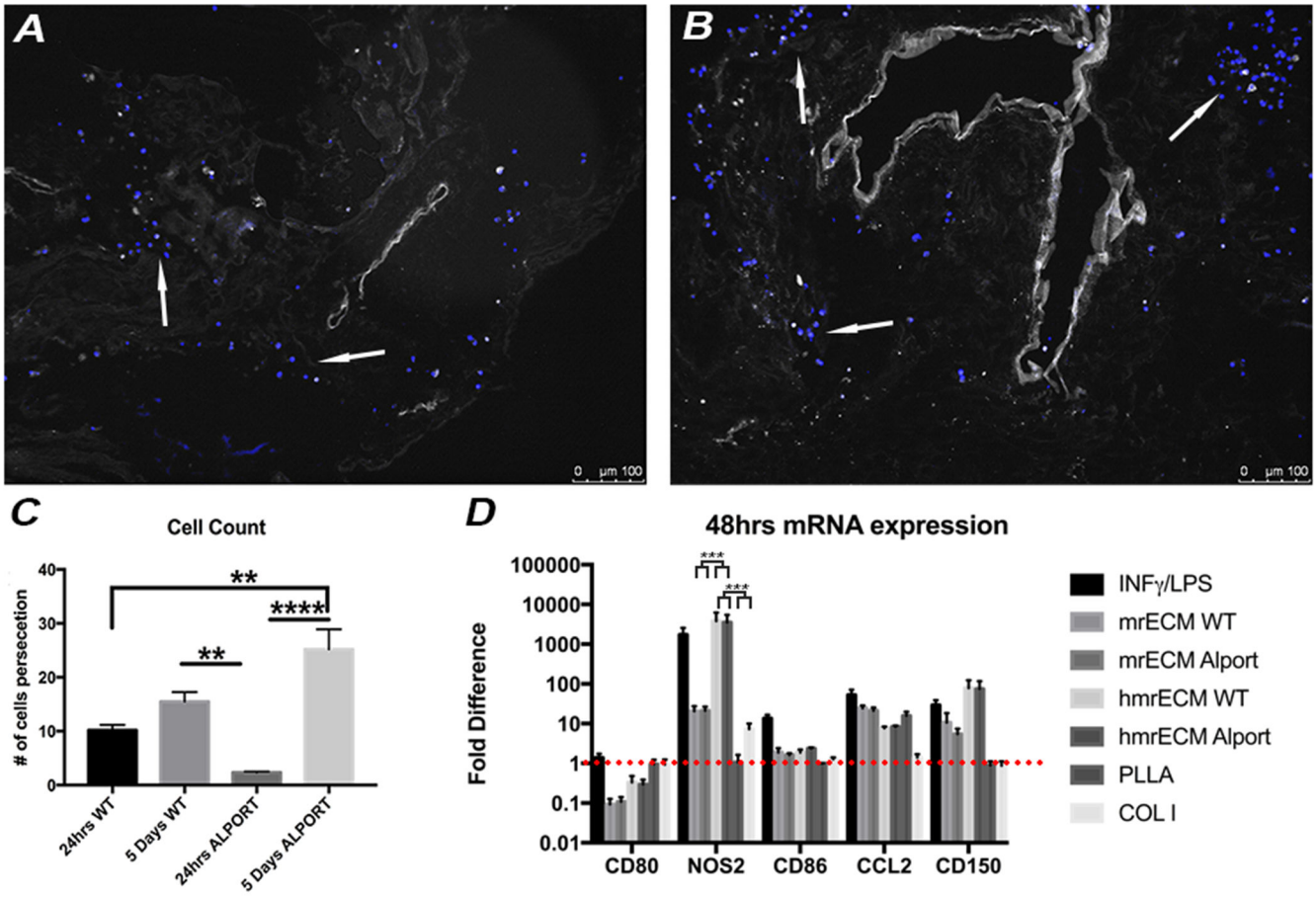


**Figure 4: Macrophage interaction with WT and Alport mrECM**

**A-B**. Representative immune fluorescence images of DAPI staining of macrophages (arrow) seeded onto 7 months mrECM derived from WT (**A**) and Alport (**B**) after for 5 days of seeding. **C**. Graph representing counting of number of macrophages adhering to WT and Alport mrECM at 24hrs and 5 days after seeding. A statistically significant increase in macrophages adhesion (quantitative expression) is observed from 24hrs to 5days in Alport but not in WT mrECM. Minimum of 60 images at 10x bright field microscopic per experimental group were counted for positive expression of DAPI (**p<0.005, ****p<0.0001). **D**) Graphs representing fold differences in mRNA expression of CD80, NOS2, CD86, CCL2, CD150 derived from macrophages stimulated with INF-γ/LPS (black column), seeded on homogenized mrECM from both WT and Alport mice and on mrECM from both WT and Alport mice or seeded on PLLA or collagen type I after 48hrs normalized to basal expression of non-stimulated TCP (represented by the red dotted line).

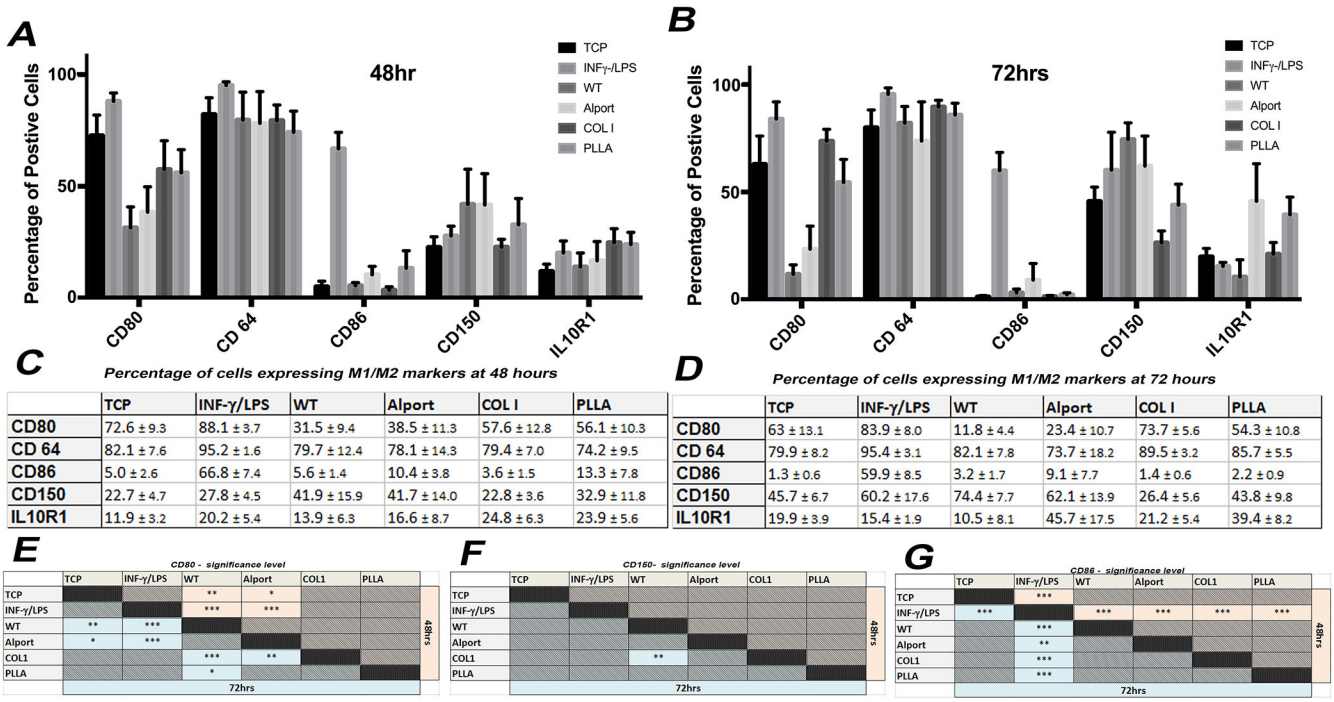


| C | TCP | INF-γ/LPS | WT | Alport | COL I | PLLA |
|---|---|---|---|---|---|---|
| CD80 | 72.6 ± 9.3 | 88.1 ± 3.7 | 31.5 ± 9.4 | 38.5 ± 11.3 | 57.6 ± 12.8 | 56.1 ± 10.3 |
| CD 64 | 82.1 ± 7.6 | 95.2 ± 1.6 | 79.7 ± 12.4 | 78.1 ± 14.3 | 79.4 ± 7.0 | 74.2 ± 9.5 |
| CD86 | 5.0 ± 2.6 | 66.8 ± 7.4 | 5.6 ± 1.4 | 10.4 ± 3.8 | 3.6 ± 1.5 | 13.3 ± 7.8 |
| CD150 | 22.7 ± 4.7 | 27.8 ± 4.5 | 41.9 ± 15.9 | 41.7 ± 14.0 | 22.8 ± 3.6 | 32.9 ± 11.8 |
| IL10R1 | 11.9 ± 3.2 | 20.2 ± 5.4 | 13.9 ± 6.3 | 16.6 ± 8.7 | 24.8 ± 6.3 | 23.9 ± 5.6 |

| D | TCP | INF-γ/LPS | WT | Alport | COL I | PLLA |
|---|---|---|---|---|---|---|
| CD80 | 63 ± 13.1 | 83.9 ± 8.0 | 11.8 ± 4.4 | 23.4 ± 10.7 | 73.7 ± 5.6 | 54.3 ± 10.8 |
| CD 64 | 79.9 ± 8.2 | 95.4 ± 3.1 | 82.1 ± 7.8 | 73.7 ± 18.2 | 89.5 ± 3.2 | 85.7 ± 5.5 |
| CD86 | 1.3 ± 0.6 | 59.9 ± 8.5 | 3.2 ± 1.7 | 9.1 ± 7.7 | 1.4 ± 0.6 | 2.2 ± 0.9 |
| CD150 | 45.7 ± 6.7 | 60.2 ± 17.6 | 74.4 ± 7.7 | 62.1 ± 13.9 | 26.4 ± 5.6 | 43.8 ± 9.8 |
| IL10R1 | 19.9 ± 3.9 | 15.4 ± 1.9 | 10.5 ± 8.1 | 45.7 ± 17.5 | 21.2 ± 5.4 | 39.4 ± 8.2 |

**Figure 5: Phenotypical analysis of macrophages seeded on mrECM (WT and Alport) or synthetic biomaterial.**

**A-B.** Graphs representing the percentage of cells positive for CD80, CD64, CD86, CD150 and IL10R1 cultured and seeded in different conditions (non stimulated-TCP, INF-γ/LPS stimulated, WT mrECM, Alport mrECM, collagen I and PLLA) after 48hrs (**A**) and 72hrs (**B**). **C-D.** Table reporting n percentage of macrophages expressing M1/M2 markers for all samples analyzed at 48hrs (**A**) and 72hrs (**B**). All values are presented as mean ± SEM. **E-G.** Tables summarizing statistical significant differences for results represented in **A-D** between the different groups at 48hrs (light red cells) and 72 hrs (light blue cells) for CD80, CD150 and CD86. No significance was evident for CD64 and IL-10R1 between the experimental groups , *p-value <0.05; **p-value <0.01; *** p-value <0.001.